



Multipurpose Additives Toward Improving the Polymer Cold Spray Process

Tristan W. Bacha^{1,2} · Francis M. Haas^{1,3} · Isaac M. Nault⁴ · Joseph F. Stanzione III^{1,2}

Submitted: 16 June 2023 / in revised form: 19 January 2024 / Accepted: 2 February 2024 / Published online: 27 March 2024
© The Author(s) 2024

Abstract Polymers have proven to be challenging to cold spray, particularly with high efficiency and quality when using inexpensive nitrogen (N₂) and air propellants. Helium (He), when used as a process propellant, can improve spray deposit properties but is often undesirable due to its limited availability and high cost. In this study, additives of multiple particle sizes and materials were mixed with polymer powder in an effort to improve the performance of polymer sprays using mainly N₂ as a process propellant. The effects of hard-phase additives on

deposit microstructure were investigated by precise ion beam polishing of deposit cross sections and subsequent electron microscope imaging. Additional metrics including the density and post-spray composition of deposits were investigated to quantify the peening effect and the amount of embedded additive. Additives, regardless of size, were observed to embed in the spray deposits. Additionally, hard-phase additives demonstrated nozzle cleaning properties that continually remove polymer fouling on the nozzle walls. Inversely, sprays with polymer powder and no additives tended to clog the nozzle throat and diverging section because of continual fouling.

Keywords cold spray · density measurement · feedstock · polymer · porosity

This article is an invited paper selected from presentations at the 2023 International Thermal Spray Conference, held May 22–25, 2023, in Québec City, Canada, and has been expanded from the original presentation. The issue was organized by Giovanni Bolelli, University of Modena and Reggio Emilia (Lead Editor); Emine Bakan, Forschungszentrum Jülich GmbH; Partha Pratim Bandyopadhyay, Indian Institute of Technology, Karaghpur; Šárka Houdková, University of West Bohemia; Yuji Ichikawa, Tohoku University; Heli Koivuluoto, Tampere University; Yuk-Chiu Lau, General Electric Power (Retired); Hua Li, Ningbo Institute of Materials Technology and Engineering, CAS; Dheepa Srinivasan, Pratt & Whitney; and Filofteia-Laura Toma, Fraunhofer Institute for Material and Beam Technology.

✉ Tristan W. Bacha
bachat9@rowan.edu

Joseph F. Stanzione III
stanzione@rowan.edu

¹ Advanced Materials and Manufacturing Institute (AMMI), Rowan University, Glassboro, NJ, USA

² Department of Mechanical Engineering, Rowan University, Glassboro, NJ, USA

³ Department of Chemical Engineering, Rowan University, Glassboro, NJ, USA

⁴ DEVCOM Army Research Laboratory ARD, Manufacturing Science and Technology Branch, Aberdeen, MD, USA

Introduction

Polymer cold spray has been of recent interest as a tool to apply corrosion barriers (Ref 1) and hydrophobic coatings (Ref 2, 3), as well as create 3D parts via additive manufacturing (Ref 4). However, the polymer spray process is far from optimal, with deposition efficiencies that are typically low (Ref 3, 5, 6), porous deposits (Ref 7, 8), and few characterizations of mechanical properties (Ref 4). To improve outcomes, modifications to the process including nozzle design (Ref 5, 9–11), particle composition (Ref 12–14), pre-heating of powders (Ref 8) and substrates (Ref 4, 5, 9, 10, 15) have been attempted in addition to adjusting basic spray parameters like system temperature and pressure (Ref 4, 5, 15). Still, deposition quality and efficiency have yet to be truly optimized.

Among the myriad of process parameters that exist, the incorporation of additives to polymer powder feedstocks is relatively unexplored. Khalkhali et al. found several

advantages when incorporating glass peening beads into polymer powder feedstocks sprayed with a low-pressure cold spray system (Ref 16). Peening media was found to widen the powder deposition window. Powder deposited at lower process gas temperatures and both higher and lower gas pressures. Additionally, the peening media reduced deposit surface roughness and improved deposition efficiency slightly. At supersonic velocities, peening media was found to embed in the deposits, but it did not at lower velocity conditions explored in that study. Ravi and several co-authors published multiple reports where nano-additives were incorporated into powder mixtures (Ref 3, 17–19). Nano-additives were demonstrated to improve deposition efficiency, which was attributed to the additives providing extra bonding sites between impacting polymer particles. Sulen et al. also found that fumed nano-alumina improved deposition efficiency in their fluoropolymer coatings (Ref 20). Tillmann and Zajackowski sprayed mixtures of polyamide 12 and alumina particles using a low-pressure cold spray system with downstream powder injection (Ref 1). Their results focused on the morphology of the final coating rather than quantifying peening or nozzle cleaning effects of the additive. However, they mentioned that the alumina was suspected to act as a peening agent while also helping to prevent the nozzle from fouling. Alumina was found to embed in the coatings, but substantial porosity was observed in the cross sections even with increasing additive content.

Although additives appear to be effective for improving the polymer cold spray process, no previous study, to our knowledge, has characterized the densification effect that is claimed to occur by incorporating an additive. Herein, the effects of several peening media on the deposit properties were studied using a high-pressure cold spray system. Additives were found to incorporate into spray deposits and provided peening action leading to deposit densification. In addition to the peening properties, additives were found to have a crucial role in spray quality/stability by acting as nozzle anti-fouling agents.

Methods and Materials

For the following powders, the particle sizes reported are nominally the diameters as reported by the manufacturer. Nylon 6 powder (AM30-PD-000155) from Goodfellow USA (55 μm avg) with a melting temperature (T_m) of 204.7 ± 0.7 °C was used for all experiments. The melting point was determined by differential scanning calorimetry using a TA Instruments Discovery DSC 2500. Samples were heated in triplicate from -50 to 250 °C twice at a rate of 10 °C/min to allow for powder to consolidate and settle in the pan. The melting point was taken as the

minimum of the melting endotherm. Additives included 63–125 μm Microblast B120 spherical blasting media (Saint-Gobain ZirPro, Le Pontet, France), 45–90 μm Ballotini glass spheres (Potters, Malvern PA), 300–425 μm Zirshot Z300 shot peening spheres (Saint-Gobain ZirPro), and < 44 μm tabular alumina with angular morphology (GNP Graystar, Amherst, NY). The Microblast (blasting media) and Zirshot (shot peening media) are hard ceramic materials consisting of a blend of ZrO_2 , SiO_2 , and Al_2O_3 . A range of sizes were selected from materials on hand to determine the effect of size on the degree to which an additive embeds. Powder blends were mixed using a Turbula 3D powder mixer for approximately 30 min. All powders were tumbled on a rolling mill in an HDPE bottle to ensure the powder was free flowing before loading into a rotary drum feeder for spraying.

Powders were sprayed on to $\frac{1}{4}$ " thick nylon 6 substrates (obtained from McMaster Carr) that were pre-treated by sanding to 320 grit and cleaned with an isopropanol wipe. A VRC Metal Systems Gen III high-pressure cold spray system was used for all sprays. Both the nitrogen (N_2) and helium (He) spray conditions were chosen based on previous work (Ref 8). The N_2 spray condition used a VRC #60 nozzle and block applicator with temperature and pressure setpoints of 150 °C and 250 psig, respectively. The rotary powder feed system was set to 14 RPM, and 50 SLM of gas flow through the feeder. Spray path control was achieved using a robot arm. The spray path consisted of 25 parallel lines spaced 2 mm apart. The pattern was repeated for a total of 12 spray layers, with an initial standoff distance from the substrate of 25.4 mm and raster speed of 100 mm/s. Between each layer, the standoff distance was increased incrementally to keep the distance consistent as the deposits grew. The amount was measured from a small spray coupon before each large spray was conducted (~ 0.5 mm per pass). During sprays, the system main gas flowrate was intermittently recorded to monitor for nozzle clogging, as further discussed below. The powder feed gas flow rate remained nearly constant at the setpoint and would only substantially decrease if the nozzle was markedly clogging. After each spray, the nozzle bore was examined for fouling and conditions of interest were photographed.

Nylon and alumina powder mixtures were sprayed with He gas using the same spray system but with a VRC #58 nozzle and a barrel applicator. System setpoint temperature and pressure were 150 °C and 300 psig, respectively, and the powder feeder was set to a rotational speed of 3.5 RPM and gas flow rate of 100 SLM. The spray path was modified so that the spacing between lines was 0.5 mm and the raster speed was 400 mm/s. A total of 40 parallel lines and 32 layers were sprayed for this condition. Small alumina particles were chosen as they were hypothesized to provide

good abrasive action to clean the nozzle walls, as some fouling was noted during preliminary experiments that showed He provided higher quality coatings than N₂. Additionally, alumina was chosen as it has been shown to form an interfacial phase with nylon 6 (Ref 21). He was not used for all additives due to cost constraints.

Powder feed rates were calculated for each spray and are summarized in Table 1. Feed rates were calculated by weighting the amount of powder in the feeder before and after spraying. The difference was divided by the total spray time to estimate the feed rate for each condition.

Velocity calculations for the powders and additives were performed using the methods of Bacha et al. (Ref 22). Velocities for select conditions were determined experimentally using a HiWatch HR (Oseir Oy, Tampere, Finland).

A Leica EM TIC 3X ion beam etching system was used to polish cross sections of select deposits. Samples were first reduced in size using a mechanical mill before mounting on the TIC. A cryogenic stage was used to keep the material cool for a milling time of 15 h at 6 kV and – 145 °C.

A Phenom XL scanning electron microscope (SEM) and FEI Nova NanoSEM 600 were used to image samples. Samples imaged in the Phenom XL were sputtered with gold using a Cressington 108 sputter coater. Images were taken at 10 kV using the backscatter (BSD) and secondary electron detectors (SED). For the NanoSEM, samples were sputtered with iridium using a Leica ACE 600 and imaged in the high vacuum mode at 5 kV with the BSD and SED.

Optical micrographs were taken with a Keyence VHX-7000 microscope. A cross section of the 40 wt.% Z300 spray was mounted in epoxy resin, using several vacuum purge cycles to infiltrate the pores with resin. After infiltration, the sample was polished using silicon carbide paper up to 1200 grit. Images of the cross sections were taken

using both coaxial lighting and ring lighting on the VHX-7000 to highlight different features of the deposit.

Sprayed samples were oxidized in a TA Instruments Discovery 550 TGA thermogravimetric analyzer to determine embedded refractory additive content. Samples were heated in air from 50 to 700 °C at a rate of 10 °C/min in platinum pans and then held isothermally at 700 °C for 10 min. Nylon was found to leave a charred residue content equal to 2.4 ± 0.1% of the original sample mass; this residue fraction was considered for the additive percentage calculations presented below. Equation 1 relates the polymer mass in the deposit (*M_p*) to the mass sampled from the deposit (*M_D*), the mass after burn-out (*M_B*) and the mass fraction of polymer that remains as charred residue (*x_c* = 0.024). Equation 2 provides the equation for determining additive mass (*M_A*) in the deposit. Mass fraction of polymer or additive was determined by dividing *M_A* or *M_p*, respectively, by *M_D*.

$$M_p = \frac{M_D - M_B}{1 - x_c} \tag{Eq 1}$$

$$M_A = M_D - M_p \tag{Eq 2}$$

Deposit (bulk) density measurements were made according to the submerged mass method (Ref 23). Sprayed samples of a known mass were coated in paraffin wax before measuring to prevent fluid ingress. Anhydrous ethanol was used as a working fluid. The density of the deposit (*ρ_d*) was defined as the volume-weighted average of the additive density (*ρ_a*) and regions of polymer and voids (*ρ_p*), with corresponding volume fractions (*y_p*) and (*y_a*) (Eq. 3). Estimates of error in calculating the density of the combined polymer/void phase are presented in Equation 4 and 5. The standard deviation of polymer/void phase (*σ_{ρ_p}*) was considered to be a function of the standard deviation for the measured deposit density (*σ_{ρ_d}*) and measured additive volume fraction (*σ_{y_a}*).

$$\rho_d = y_p \rho_p + y_a \rho_a \tag{Eq 3}$$

$$\sigma_{\rho_p}^2 = \left(\frac{\partial \rho_p}{\partial \rho_d}\right)^2 \sigma_{\rho_d}^2 + \left(\frac{\partial \rho_p}{\partial y_a}\right)^2 \sigma_{y_a}^2 \tag{Eq 4}$$

$$\sigma_{\rho_p}^2 = \left(\frac{1 - y_a}{\left(1 - y_a \frac{\rho_a}{\rho_d}\right)^2}\right)^2 \sigma_{\rho_m}^2 + \left(\frac{\rho_a \rho_d (\rho_d - \rho_a)}{(\rho_a - \rho_d y_a)^2}\right)^2 \sigma_{y_a}^2 \tag{Eq 5}$$

The adhesion/cohesion strength of select additive blends were examined by and prepared according to the ASTM C633-13 test method (Ref 24). Threaded testing rods were machined from nylon 6 rod stock (obtained from MSC Direct) and the top surface was sprayed directly on to after

Table 1 Flow rates of powder as-measured for each spray condition

Gas	Powder	Rate, g/min
N ₂	Nylon	6.29
N ₂	10 wt.% Glass + Nylon	5.07
N ₂	20 wt.% Glass + Nylon	6.82
N ₂	40 wt.% Glass + Nylon	7.52
N ₂	20 wt.% B120 + Nylon	5.19
N ₂	10 wt.% Z300 + Nylon	5.38
N ₂	20 wt.% Z300 + Nylon	6.95
N ₂	40 wt.% Z300 + Nylon	6.49
He	Nylon	1.84
He	20 wt.% Alumina + Nylon	1.93

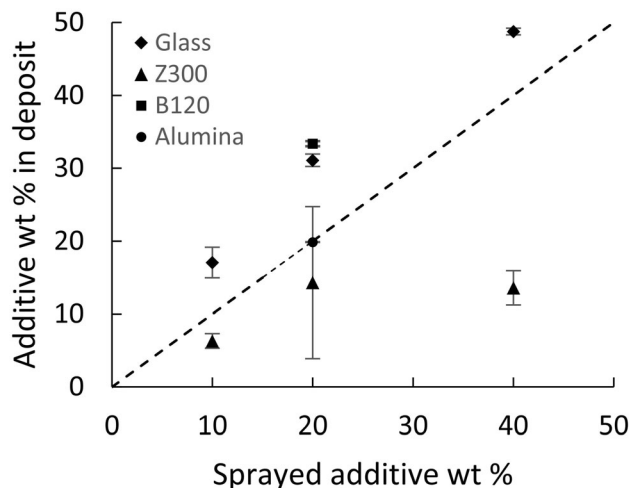


Fig. 1 Weight percent of additive remaining in sprayed deposit determined by thermogravimetric analysis for glass beads (45–90 μm), Z300 media (300–425 μm), B120 (63–125 μm) and alumina (< 44 μm). The dashed line was plotted with a slope of 1 for reference

sanding and cleaning. Spray parameters were used as described previously, except only 6 layers were sprayed. The coated test specimens were then glued with J-B Weld epoxy to another threaded rod to complete the test fixture. The testing was performed on an Instron 5966 load frame with a 10 kN load cell. Samples were subject to tension at a crosshead travel rate of 0.02 mm/s until failure. The force at break was recorded for analysis. Four samples were tested unless otherwise noted.

Results and Discussion

Peening Effects on Deposit Composition and Density

In each case that an additive was sprayed with nylon 6, some additive embedded in the cold spray deposit. The additive content in the final deposit versus the mixed content is given in Fig. 1 for the glass bead and Z300 additive mixtures. In general, the glass beads embedded readily in the deposit, resulting in a composition richer in additive than the as-mixed powder blends (i.e., enrichment of additive). The larger Z300 particles, when mixed in the same mass proportions as the glass, resulted in less overall embedding than the glass (i.e., additive depletion). This is attributed to the Z300 particles being much larger at a size range of 300–425 μm compared to the 45–90 μm glass. Smaller particles impact at higher velocities (summarized in Table 2) resulting in a condition that favors penetration into the deposit. The 20 wt.% Microblast B120 formed deposits with a weight percentage of $33.4 \pm 0.35\%$, similar to the glass sample. The small (< 44 μm) 20 wt.% alumina powder produced deposits with an additive content

Table 2 Predicted impact velocity (v_{pi}) and density for each condition with select particle sizes for each spray as references

Gas	Particle	Size, μm	v_{pi} , m/s	ρ , kg/m^3
He	Nylon	55*	1001	1130
He	Alumina	44	809	3525
He	Alumina	20†	997	3525
He	Alumina	5†	1320	3525
N ₂	Nylon	55*	521	1130
N ₂	B120	63	425	3800
N ₂	B120	125	362	3800
N ₂	Glass	45	488	2450
N ₂	Glass	90	430	2450
N ₂	Z300	300	277	3800
N ₂	Z300	425	245	3800

Velocities were predicted using the methods described elsewhere (Ref 7, 8). All densities were retrieved from the manufacturer, except for the glass particles which were determined experimentally.

*Average reported particle size.

†Arbitrary particle sizes chosen as additional reference points (reported to be a size range < 44 μm).

of $19.9 \pm 0.05\%$, indicating that the mixture components deposited with nearly equal efficiency.

The glass, B120, and alumina mixtures were observed to form homogeneous mixtures upon initial mixing in storage bottles by vigorously shaking. Conversely, the Z300 particles were observed to demix from the main nylon phase, resulting in stratification into two layers. This resulted in feed irregularities that caused the uncertainty evident in the 20 wt.% Z300 sprays. For future experiments with large dense additive particles, separate powder feeders are recommended for better control of the mixture to avoid the demixing issue that was observed.

The embedding of particles resulted in increases in overall density of the deposits with increasing additive content as depicted in Fig. 2(a). When the deposit density was adjusted for the additive content (giving a density of only the polymer and void fractions, denoted as ρ_p in the methods section), the peening action of the additives becomes apparent as shown in Fig. 2(b). Although there is substantial uncertainty (determined from the propagation analysis in the methods section), nearly all the loadings of additive resulted in increasing density with additive content over the sprays with pure nylon in their respective gases (0 wt.% additive in both N₂ and He). Note that density appears to decrease from the 20 to 40 wt.% Z300; however, this may be attributable to feed rate irregularities that resulted in a greater number of peening particles being sprayed (and depositing) as reflected by the uncertainties shown in Fig. 1. The adjusted density of the 20 wt.% alumina spray was observed to decrease slightly compared

Fig. 2 (a) Measured density (ρ_d) of the as-deposited samples including polymer and additive. (b) Adjusted density (ρ_p) of the deposits estimating only the polymer and void space deposit fraction

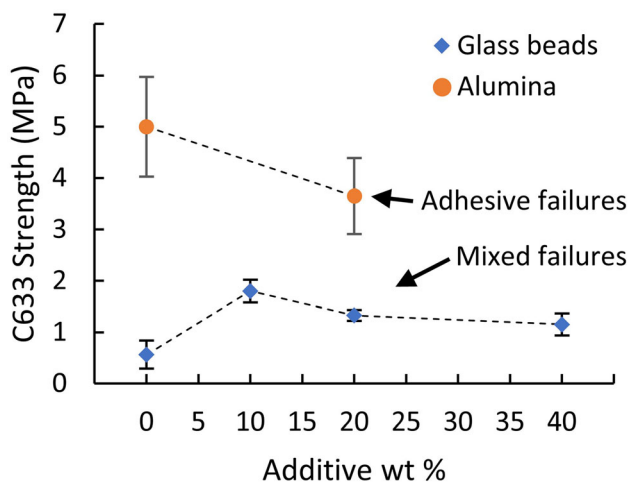
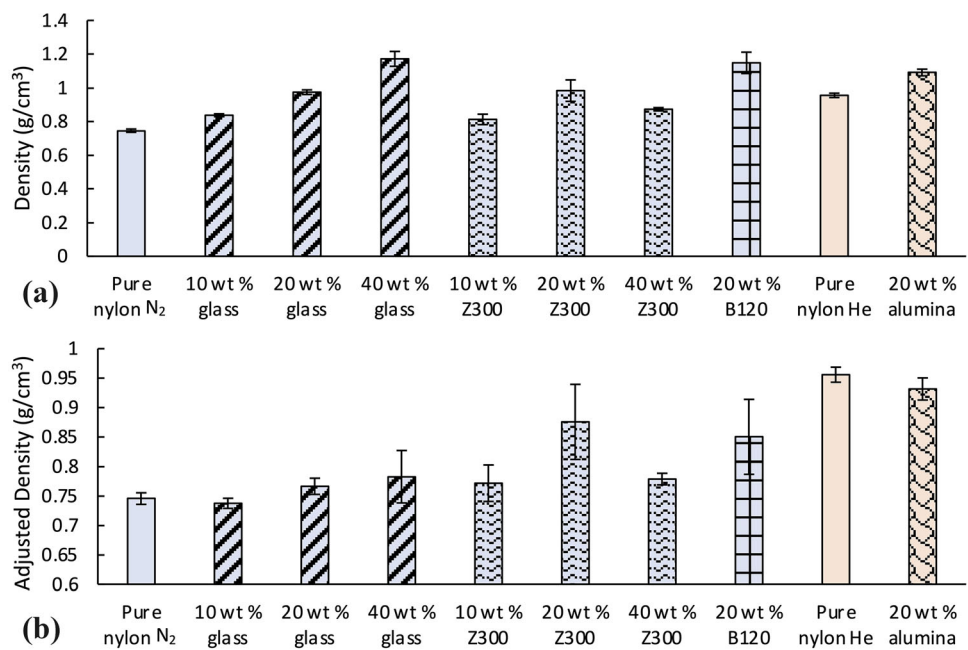


Fig. 3 ASTM-C633 testing results for additive sprays with glass beads (N₂ propellant) and alumina (He propellant). Additive concentration is the as-sprayed wt.% of the powder mixture. Note that only 2 samples were tested for the 10 wt.% glass sample

to the pure nylon sprayed with helium. This is likely due to penetrating action of the small alumina particles, rather than peening and densification action on the deposit. As shown in Table 2, the largest alumina particles were smaller than the average nylon powder particle size.

Peening Effects Measured by ASTM-C633 Mechanical Testing

A set of samples containing glass and alumina were tested using the ASTM C633 methodology. The results of four

tests using N₂ propellant and two using He propellant are depicted in Fig. 3.

The pure nylon sprays benefitted from nearly a 9-fold increase in C633 strength when the spray gas was changed from N₂ to He. Notably, failure in the He-sprayed samples was purely adhesive failure between the deposit and substrate, while the N₂-sprayed samples exhibited a mixture of adhesive and cohesive failures. Thus, the deposit cohesive strength may be considerably higher than reported above. The decrease in adhesive strength when increasing from 0 to 20 wt.% alumina content appears to be due to alumina particles crowding the particle substrate interface. This idea is expanded upon in the following section with SEM micrographs.

When glass additive was incorporated in the nylon spray, the adhesion/cohesion strength increased greater than 2x for all additive loadings. This may be partially attributed to slight densification of the deposit and a subsequent improvement in mechanical strength. Furthermore, the glass beads were found to have a cleaning action on the nozzle bore. This cleaning action ultimately kept the nozzle throat and converging section clean, leading to higher particle velocities throughout a spraying operation. This is discussed further in the later section on nozzle fouling.

Microstructural Analysis of Deposits

Several SEM images of select deposits were taken to further understand the effects of each additive on deposition. In Fig. 4(a), (b), and (c), cross sections of deposits after ion beam milling are shown. Ion beam milling was chosen to remove a final layer from mechanically cross-sectioned

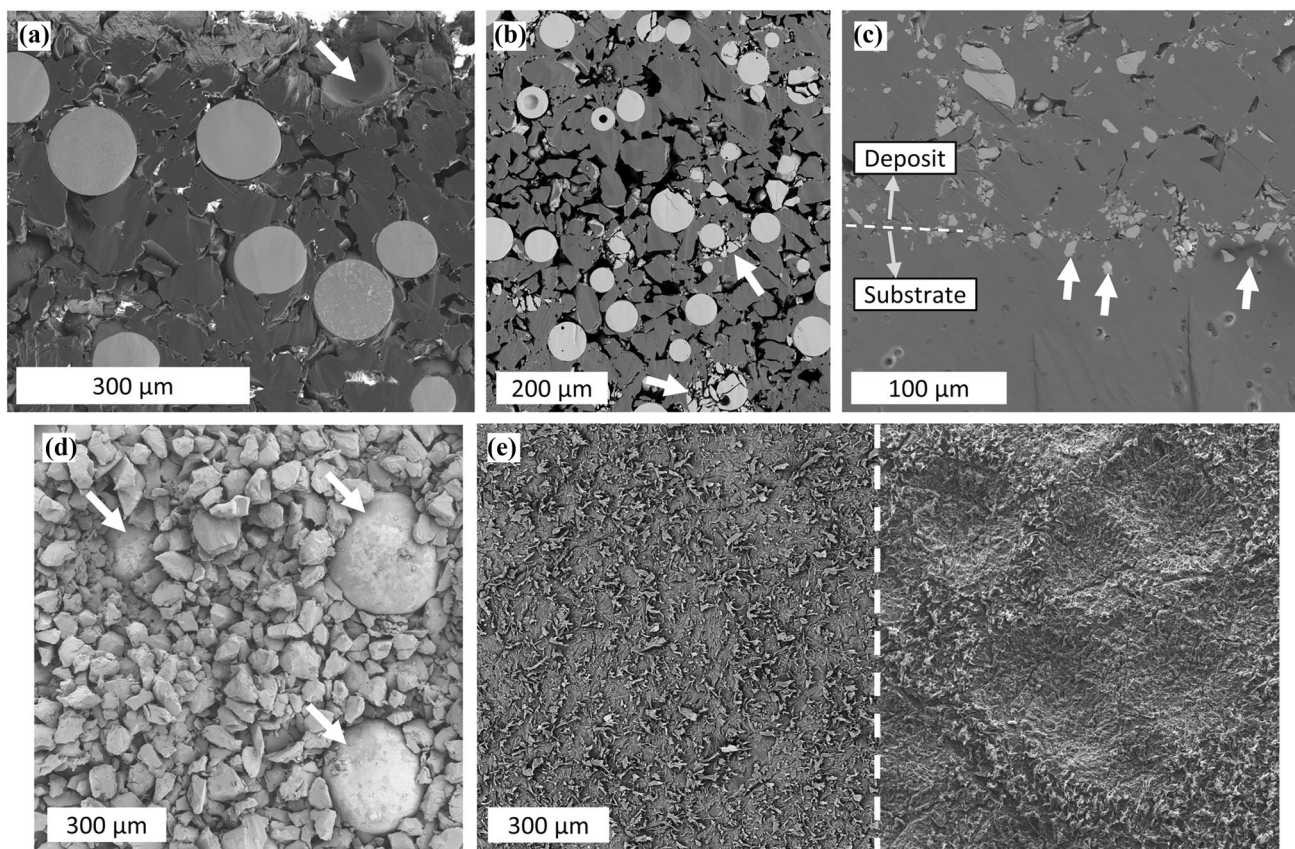


Fig. 4 (a) Ion-milled cross section of a spray with 20 wt.% B120. The white arrow indicates a crater from a dislodged particle. (b) Ion-milled cross section of the 40 wt.% glass spray. The white arrows highlight peening particles damaged from subsequent impacts. (c) Ion-milled cross section of the 20 wt.% alumina spray with He carrier gas. The white arrows point to alumina particles that

penetrated the substrate. The dashed line and gray arrows indicate the particle/substrate boundary. (d) Z300 particles attached to the spray surface are highlighted by white arrows. (e) A substrate as-prepared (left) and after peening with neat Z300 particles (right). No embedding occurred in the dense substrate. (Pictures (a), (b), and (c) were taken with the NanoSEM 600; (d) and (e) with Phenom XL)

samples to preserve the true structure of the deposit and minimize any chances for dislodging of additives from the cross section during preparation. Manual sectioning may lead to additive pull out and the creation of void spaces post-spray (Ref 25). Figure 4(a) depicts B120 additives (light circles) embedded in the deposit. Also visible is a crater left behind by a dislodged particle, emphasizing the deformation that additives have the potential to induce. Many embedded particles in deposits were shown previously (Fig. 2) to increase the overall density of the deposit and have a compacting effect on the polymer. However, a drawback to additive embedding is exemplified in the deposit formed by the 40 wt.% glass mixture (Fig. 4b). With a high concentration of additive, particles are more likely to undergo repeat impacts that can cause fracturing of embedded particles. These defects detract from the potential for mechanical property improvements, as shown in Fig. 3 for higher additive blend fractions. Although not apparent in Fig. 4(a), B120 additives were also susceptible to fracturing from repeat impacts, although this was less

probable due to their lower concentration and impact resistance as claimed by the manufacturer.

The adhesive strength decrease observed in the 20 wt.% alumina spray (Fig. 3) is attributed to a disrupted interface between nylon particles and the nylon substrate. Figure 4(c) shows concentration of alumina particles at the particle/substrate interface. It is hypothesized that the high velocity, density, and small size of the alumina particles enables them to deposit more effectively onto/into the substrate than the nylon particles. During formation of the initial layer, the substrate is relatively cool and hard as it has had limited exposure to the hot gas jet. The small particles are seen to easily embed into the cool substrate. Examples of this embedding are highlighted with white arrows in Fig. 4(c). Although the interface became crowded with alumina particles, the reduction of voids apparent in Fig. 4(c) when compared to Fig. 4(b) is attributed to the higher velocity He spray condition. Less void space implies more particle-particle contact, resulting in enhanced mechanical properties. This is reflected in Fig. 3, where the

alumina + nylon powder sprayed with He failed adhesively at much higher forces than the cohesive failures of the glass + nylon powder sprayed with N_2 .

The larger Z300 particles tended to embed less than the glass particles as implied in Fig. 1. However, these particles still embedded even with a lower inferred impact velocity and average nominal diameter greater than 5x the nylon material. Figure 4(d) shows three Z300 particles embedded in the surface of a deposit, as indicated by white arrows in Fig. 4. The large particles appear to inhibit the deposition of nylon on top of them. The top left Z300 particle has a crater-like formation of nylon particles depositing on top of it, suggesting that such formations may lead to defects above embedding Z300 particles, detracting from deposit quality compared to a case where the particles exclusively rebounded. No ion-milled cross sections were obtained for the Z300 spray as milling was impractical due to the low material removal rate and large size of the Z300 particles. Instead, a section from the 40 wt.% Z300 spray was taken and mounted in epoxy for viewing under an optical microscope. Images of the cross section from optical microscopy are given in Fig. 5.

Figure 5 shows several embedded particles in a cross section of the 40 wt.% Z300 spray. A clip used for support during resin mounting and the epoxy are highlighted in the micrograph ((5) and (6), respectively). Most of the particles have compact regions of nylon deposit beneath them, suggesting successful densification of the underlying deposit ((1) in Fig. 5a). An exception is highlighted by (2) in Fig. 5(a), where an area of infiltrated epoxy is observed below the embedded particle. Although a void is present, the particle likely embedded itself into a defect and caused some densification, evidenced by contours in the adjacent

deposit that match the particle's shape. The large percentage of embedded Z300 by examining the deposit beyond the cross-sectioned layer. The coaxially illuminated optical image of Fig. 5(b) reveals more particles embedded throughout the deposit (indicated by (3)).

Although substantial embedding was observed into the deposited nylon material, no embedding was observed when purely Z300 was sprayed on to a nylon substrate at the same spray parameters. Figure 4(e) shows an as-prepared substrate (left) compared to a substrate impacted by the peening particles. On the fully dense substrate, the relatively low velocity Z300 particles results in a peening effect and complete rebound. Conversely, the cold sprayed deposits with lower bulk densities and higher porosities are susceptible to a greater degree of penetration. Many particles are decelerated and become trapped in the deposit such that few rebounds occur.

Anti-fouling Effect of Hard-Phase Additives

Additives were found to have substantial effects on reducing nozzle fouling during sprays. Figure 6(a) shows a clean nozzle before spraying neat nylon with N_2 propellant. After a spray, the nozzle bore became contaminated with adhered nylon particles and residue, as shown by the reduced reflection and apparent irregularities in Fig. 6(b). Notably, the velocities of particles as determined by the HiWatch early in the spray operation dropped by approximately 12% after spraying. When glass was incorporated as an additive, the fouling apparent in the nozzle was drastically reduced (Fig. 6c). The nozzle cleaning action and higher velocity when clean are attributed to the increase of mechanical strength observed in Fig. 3 with the

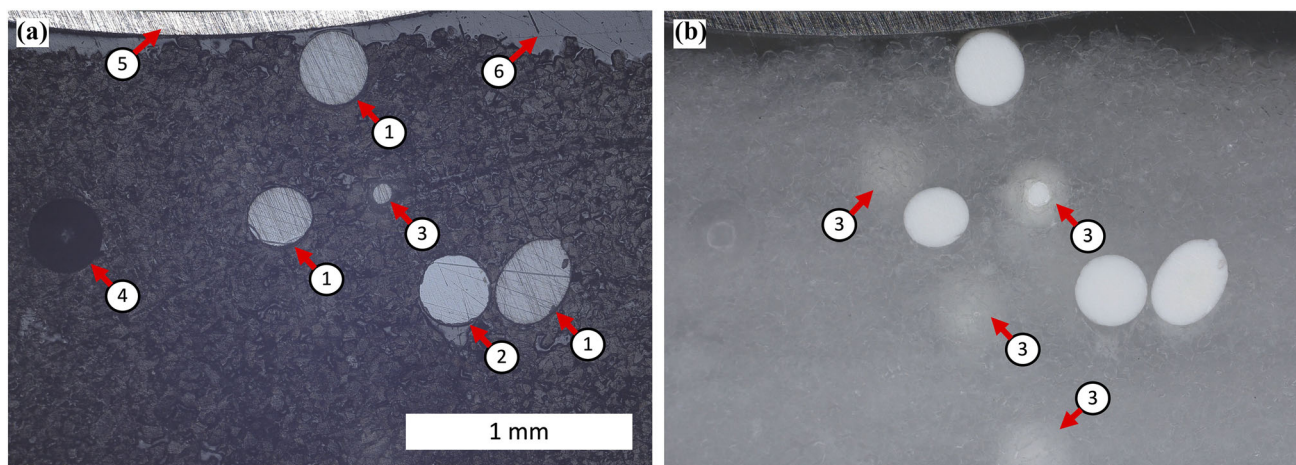


Fig. 5 Optical micrograph of the 40 wt.% Z300 spray taken using ring lighting (a) and coaxial lighting (b). Embedded particles with a dense region underneath are indicated by (1). A particle with a void underneath is indicated by (2). Particles embedded in a plane past the

cross section are indicated by (3). (4) A void space left by an embedded particle that dislodged during the polishing process. A support for resin mounting and the epoxy are denoted by (5) and (6), respectively

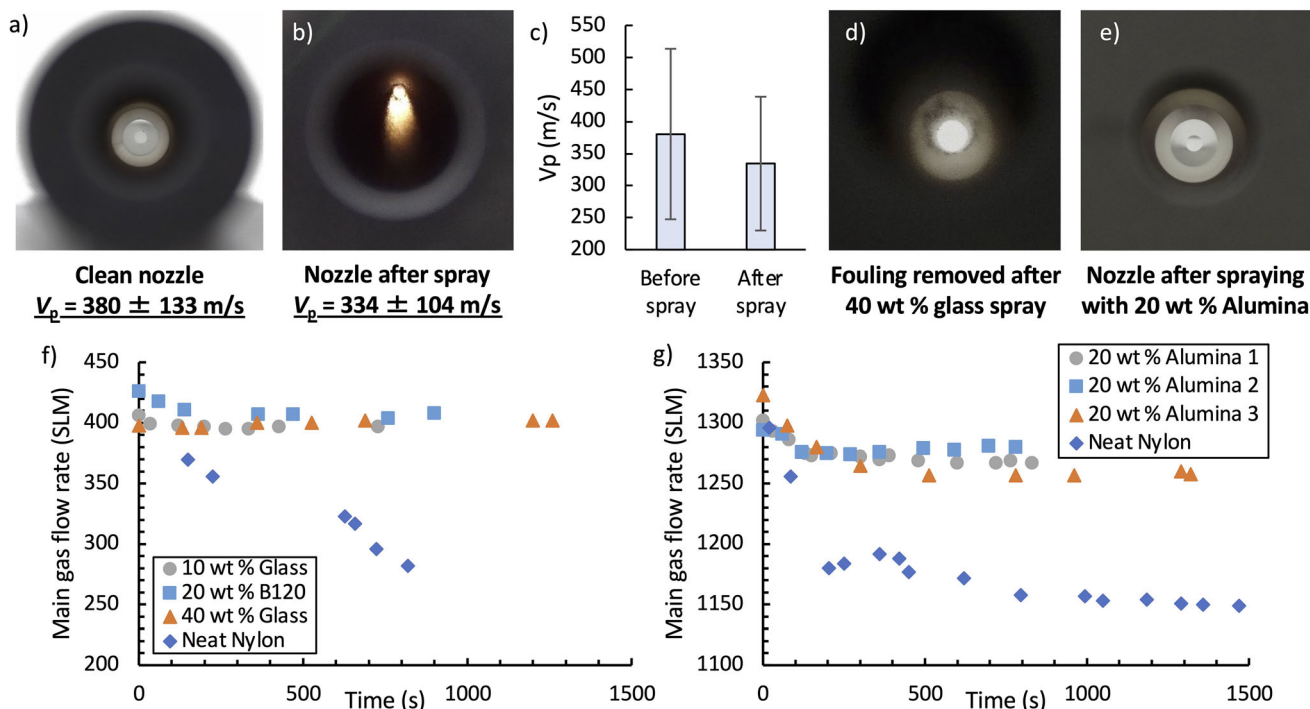


Fig. 6 (a) A clean nozzle before spraying nylon, and the average velocity determined by velocimetry at the start of the spray. (b) The same nozzle after spraying and the corresponding velocity recorded at the end of the spray. (c) Plot visualizing velocity measurements from insets (a) and (b). (d) A previously dirty nozzle cleaned after spraying

addition of glass beads. When alumina was incorporated in the He sprays, the nozzle bore was nearly spotless.

Nozzle fouling is particularly undesirable because of the reduction in spray system performance/consistency it causes. This is visualized in Fig. 6(f) and (g) when the system main gas flow rate is plotted against time for various additive and pure polymer sprays. Pure polymer sprays were difficult to accomplish, as successfully completing a spray operation was not possible every time without clogging. Figure 6(e) shows an example of an interrupted spray operation, wherein a steady decline in the main gas flow rate when spraying with neat nylon was observed. This would result in complete nozzle clogging if the spray was continued, or poorer spray performance at minimum. With additive, the main gas flow rates were essentially steady, and sprays were easily accomplished without clogging. The same issues occurred when spraying with He, although complete clogging seemed to be more difficult. Higher velocity particles induced a cleaning action in the He spray, but when additive was incorporated the cleaning action was substantially increased. The anti-fouling properties of alumina are evident across multiple sprays with the same mixture (Alumina 1, 2, and 3 in Fig. 6g). The system flow rate remained nearly constant during each spray. Minor variations in flow rate between

with a mixture of 40 wt.% glass particles. (e) A nozzle after spraying with 20 wt.% alumina and He gas. (f) Flow rates of the main process gas recorded during select sprays in N₂ gas. (g) System gas flow rates for several sprays with He carrier gas

sprays are attributed to slight leaks in the system due to connecting and reconnecting pieces of equipment.

Future Directions for Additives in Polymer Cold Spray

The ability of additives to improve deposit density and mechanical properties and stabilize spray performance demonstrated herein makes them an attractive option for future study. Based on our results, recommendations for future studies are as follows:

1. Additives show potential for peening and densification effects on deposits; however, a substantial amount of embedding occurred which may not be desired, based on the application. Additive embedding may be particularly detrimental if a large portion of additives in the deposit influence void formation or detract from the deposit cohesive strength. Numerical modeling can be used for initial screening of materials to find regimes that do not result in bonding, but provide some degree of plastic deformation of the substrate to enhance peening action (Ref 26). Additionally, different qualities of coating may respond better to additive treatment. For example, embedding may greatly reduce if the spray parameters result in naturally

denser deposits. This is supported by the result shown in Fig. 4(e) where no Z300 additive deposited on the dense substrate. Thus, finding an optimal spray condition would be beneficial before attempting to determine the optimal composition of an additive.

2. The optimal additive size/density for a given application should be determined in a separate study. Polymer peening additives may be a worthwhile avenue to study in lieu of the dense inorganic additives studied herein. Large polymer beads may impart enough energy for densification but embed less readily. Chemistries could be chosen such that the peening polymer and the to-be-deposited material are incompatible to further reduce embedding.
3. Herein, spray conditions were kept identical within the types of spray gas used. Additives may enable the use of higher spray temperatures in high-pressure cold spray systems than used for our experiments. Gas temperatures greater than the melting point of the spray material were used by Tillmann and Zajackowski (Ref 1) in their downstream injection cold spray system. In their experiments, fouling was not an issue, which is attributed to the incorporation of alumina particles. We tested the 40 wt.% Z300 spray mentioned in this work at a higher gas setpoint temperature of 200 °C, which quickly led to nozzle clogging. Although this condition failed, exploring the limits of other additives or changing variables in combination with temperature (e.g., lowering the powder feed rate to reduce clogging) is worthwhile studied.

Conclusions

The effect of several spray additives on deposit density, adhesion/cohesion strength, and nozzle anti-fouling capability was investigated in a set of polymer cold spray experiments. Larger additives were found to improve the bulk density of deposits in part due to embedding, but also appeared to densify the regions of polymer and void spaces. The densification action increased with the amount of additive used in the spray. In addition to peening action, the smaller additives exhibited nozzle anti-fouling properties that prevented clogging and stabilized the cold spray process. In turn, clean nozzles were shown to give higher particle velocities than fouled nozzles. Additives were found to both improve and detract from deposit adhesion/cohesion strength, depending on the spray condition. Small alumina additives were found to reduce deposit adhesive strength by interfering with the particle/substrate interface. Larger additives showed promise in improving deposit strength due to nozzle cleaning effects and peening

action, but at higher concentrations the benefit diminished due to fracturing behavior and a large degree of embedding. Future works investing additive size and composition are recommended due to the potential highlighted herein to improve spray quality.

Acknowledgments This research was supported by Army Research Laboratory contract W911NF-19-2-0152 and W911NF-21-2-0071. The views and conclusions contained in this document are those of the authors and should not be interpreted as representing the official policies, either expressed or implied, of the U.S. Army Research Laboratory or the U.S. Government. The U.S. Government is authorized to reproduce and distribute reprints for Government purposes notwithstanding any copyright notation herein. The authors are thankful to Scott Walck, William Gamble, Adolfo Blassino, and Nick Sotiropoulos of Army Research Laboratory for discussions and assistance regarding this work.

Funding Open access funding provided by Rowan University.

Open Access This article is licensed under a Creative Commons Attribution 4.0 International License, which permits use, sharing, adaptation, distribution and reproduction in any medium or format, as long as you give appropriate credit to the original author(s) and the source, provide a link to the Creative Commons licence, and indicate if changes were made. The images or other third party material in this article are included in the article's Creative Commons licence, unless indicated otherwise in a credit line to the material. If material is not included in the article's Creative Commons licence and your intended use is not permitted by statutory regulation or exceeds the permitted use, you will need to obtain permission directly from the copyright holder. To view a copy of this licence, visit <http://creativecommons.org/licenses/by/4.0/>.

References

1. W. Tillmann and J.F. Zajackowski, Investigation of Low-Pressure Cold-Gas Dynamic Spraying of Polyamide-12 (PA12) on Steel Surfaces, *IOP Conf. Ser.: Mater. Sci. Eng.*, 2019, **480**, p 012009.
2. A. Gibas, A. Baszczuk, M. Jasiorski, and M. Winnicki, Prospects of Low-Pressure Cold Spray for Superhydrophobic Coatings, *Coatings*, 2019, **9**(12), p 829.
3. K. Ravi, W.L. Sulen, C. Bernard, Y. Ichikawa, and K. Ogawa, Fabrication of Micro-/Nano-Structured Super-Hydrophobic Fluorinated Polymer Coatings by Cold-Spray, *Surf. Coat. Technol.*, 2019, **373**, p 17-24.
4. Z. Khalkhali and J.P. Rothstein, Characterization of the Cold Spray Deposition of a Wide Variety of Polymeric Powders, *Surf. Coat. Technol.*, 2020, **383**, 125251.
5. T.B. Bush, Z. Khalkhali, V. Champagne, D.P. Schmidt, and J.P. Rothstein, Optimization of Cold Spray Deposition of High-Density Polyethylene Powders, *J. Therm. Spray Technol.*, 2017, **26**(7), p 1548-1564.
6. Y. Xu and I.M. Hutchings, Cold Spray Deposition of Thermoplastic Powder, *Surf. Coat. Technol.*, 2006, **201**(6), p 3044-3050.
7. T.W. Bacha, D.A. Brennan, Ü. Tiitma, F.M. Haas, and J.F. Stanzione, Effects of Powder Feedstock Pre-Heating on Polymer Cold Spray Deposition. Int'l Thermal Spray Conf and Expo (ITSC 2022), May 4-6, 2022 (ASM International, Vienna, Austria, 2022), p 44-55

8. T.W. Bacha, D.A. Brennan, Ü. Tiitma, I.M. Nault, F.M. Haas, and J.F. Stanzione, Effects of Powder Feedstock Pre-heating on Polymer Cold Spray Deposition, *J. Therm. Spray Technol.*, 2023, **32**(2-3), p 488-501.
9. A.S. Alhulaifi, G.A. Buck, and W.J. Arbegast, Numerical and Experimental Investigation of Cold Spray Gas Dynamic Effects for Polymer Coating, *J. Therm. Spray Technol.*, 2012, **21**(5), p 852-862.
10. Z. Leclerc, L.E. McMunn, A. Nastic, R.N. Ben, and B. Jodoin, Manufacturing and Icephobic Performance Evaluation of Cold-Sprayed Adhesive Perfluoroalkoxy Alkane Coatings, *J. Therm. Spray Technol.*, 2023, **32**, p 851-876.
11. C.A. Bernard, H. Takana, O. Lame, K. Ogawa, and J.Y. Cavallé, Influence of the Nozzle Inner Geometry on the Particle History During Cold Spray Process, *J. Therm. Spray Technol.*, 2022, **31**(6), p 1776-1791.
12. M. Huang, Y. Liu, Z. Khalkhali, A. Kim, W. Hu, J.H. Lee, J.P. Rothstein, J. Klier, and J.D. Schiffman, Epoxy Resin-Encapsulated Polymer Microparticles for Room-Temperature Cold Sprayable Coatings, *ACS Appl. Mater. Interfaces*, 2021, **13**(42), p 50358-50367.
13. A. Gangineri Padmanaban, T.W. Bacha, J. Muthulingam, F.M. Haas, J.F. Stanzione III., B. Koohbor, and J.H. Lee, Molecular-Weight-Dependent Interplay of Brittle-to-Ductile Transition in High-Strain-Rate Cold Spray Deposition of Glassy Polymers, *ACS Omega*, 2022, **7**(30), p 26465-26472.
14. J. Muthulingam, A.G. Padmanaban, N.K. Singh, T.W. Bacha, J.F. Stanzione III., F.M. Haas, R. Jha, J.H. Lee, and B. Koohbor, Molecular Weight Controls Interactions between Plastic Deformation and Fracture in Cold Spray of Glassy Polymers, *ACS Omega*, 2023, **8**(4), p 3956-3970.
15. Z. Khalkhali, W. Xie, V.K. Champagne, J.H. Lee, and J.P. Rothstein, A Comparison of Cold Spray Technique to Single Particle Micro-Ballistic Impacts for the Deposition of Polymer Particles on Polymer Substrates, *Surf. Coat. Technol.*, 2018, **351**, p 99-107.
16. Z. Khalkhali, K.S. Rajan, and J.P. Rothstein, Peening Effect of Glass Beads in the Cold Spray Deposition of Polymeric Powders, *J. Therm. Spray Technol.*, 2020, **29**(4), p 657-669.
17. K. Ravi, T. Deplancke, K. Ogawa, J.Y. Cavallé, and O. Lame, Understanding Deposition Mechanism in Cold Sprayed Ultra High Molecular Weight Polyethylene Coatings on Metals by Isolated Particle Deposition Method, *Addit. Manuf.*, 2018, **21**, p 191-200.
18. K. Ravi, Y. Ichikawa, T. Deplancke, K. Ogawa, O. Lame, and J.Y. Cavaille, Development of Ultra-High Molecular Weight Polyethylene (UHMWPE) Coating by Cold Spray Technique, *J. Therm. Spray Technol.*, 2015, **24**(6), p 1015-1025.
19. K. Ravi, Y. Ichikawa, K. Ogawa, T. Deplancke, O. Lame, and J.Y. Cavaille, Mechanistic Study and Characterization of Cold-Sprayed Ultra-High Molecular Weight Polyethylene-Nano-ceramic Composite Coating, *J. Therm. Spray Technol.*, 2015, **25**, p 160-169.
20. W.L. Sulen, K. Ravi, C. Bernard, Y. Ichikawa, and K. Ogawa, Deposition Mechanism Analysis of Cold-Sprayed Fluoropolymer Coatings and Its Wettability Evaluation, *J. Therm. Spray Technol.*, 2020, **29**, p 1643-1659.
21. Y. Matsuda, K. Okuda, and S. Tasaka, Interfacial Phase of Nylon 6 Strongly Adsorbed on Alumina Particles, *Polym. J.*, 2020, **52**(9), p 1121-1127.
22. T.W. Bacha, N.K. Singh, I.M. Nault, B. Koohbor, F.M. Haas, and J.F. Stanzione, Thermal Gradients Govern Impact Dynamics in Thermoplastic Polymer Cold Spray, *J. Therm. Spray Technol.*, 2021, **30**(8), p 2034-2049.
23. B.C. Punmia, A. Kumar Jain, and A. Kumar Jain, *Chapter 3: Determination of Index Properties, Soil Mechanics and Foundations*, 16th ed. Laxmi Publications, 2005, p 756
24. Standard Test Method for Adhesion or Cohesion Strength of Thermal Spray Coating, ASTM C633-13, ASTM International, 2017
25. V. Bortolussi, B. Figliuzzi, F. Willot, M. Faessel, and M. Jeandin, Electrical Conductivity of Metal-Polymer Cold Spray Composite Coatings onto Carbon Fiber-Reinforced Polymer, *J. Therm. Spray Technol.*, 2020, **29**(4), p 642-656.
26. N.K. Singh, K.Z. Uddin, J. Muthulingam, R. Jha, and B. Koohbor, A Modeling Study of Bonding Mechanisms Between Similar and Dissimilar Materials in Cold Spraying on Polymeric Substrates, *J. Therm. Spray Technol.*, 2022, **31**(3), p 508-524.

Publisher's Note Springer Nature remains neutral with regard to jurisdictional claims in published maps and institutional affiliations.